ELSEVIER

Journal of Power Sources 63 (1996) 157–165

JOURNAL OF POWER SOURCES

Simulation of temperature-compensated voltage limit curves for aerospace Ni–Cd batteries using a first principles' model

B.V. Ratnakumar, P. Timmerman, S. Di Stefano

Jet Propulsion Laboratory, California Institute of Technology, 4800 Oak Grove Drive, Pasadena, CA 91109, USA

Received 2 April 1996; revised 19 June 1996

Abstract

Temperature-compensated voltage limits (*V/T* limits) are routinely used in Low Earth Orbit (LEO) satellites to permit fast charging of the Ni–Cd battery with minimum overcharge and without the problems of thermal runaway during overcharge. The voltage limits are experimentally determined from extensive testing of cells for a proper design of the charge control system to achieve the desired charge/discharge ratio in orbit. Here, we demonstrate the use of first-principles', mathematical models to construct the *V/T* curves theoretically. The predicted charge/discharge ratios under various orbit conditions such as different states of charge, in-rush currents and temperatures are compared with the experimental data.

Keywords: Batteries; Nickel; Cadmium; Voltage limits; Temperature; Mathematical models

1. Introduction

Nickel–cadmium cells may sustain thermal run-away under extreme conditions of overcharge, especially at high charge rates. Even constant voltage charging, e.g. on the Orbiting Astronomical Observatory (OAO) spacecraft, resulted in a thermal run-away. This is a result of the exothermicity of the overcharge reactions in an Ni–Cd cell (Fig. 1 [1]). The measurements from an isothermal flow calorimeter of the heat evolved on a repetitive cycling of a 6 Ah Ni–Cd

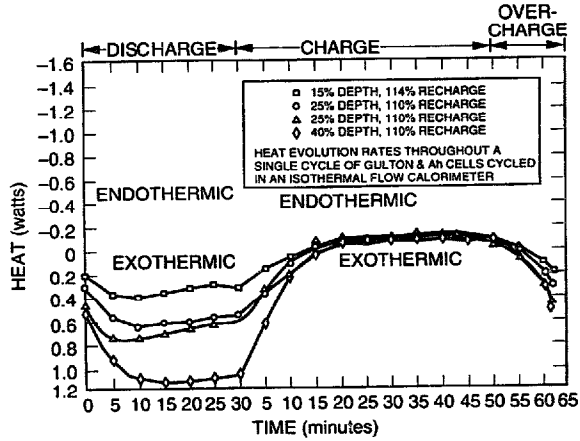

Fig. 1. Heat evolved on repetitive cycling of a 6 Ah Ni–Cd cell, measured with an isothermal flow calorimeter. (Reprinted from Ref. [1].)

PII S0378-7753(96)02444-5

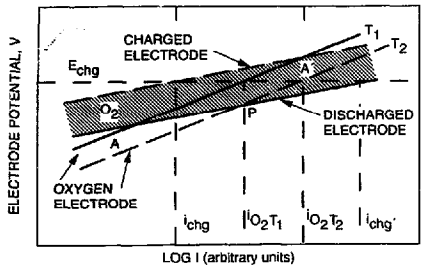

Fig. 2. Polarization curves for the charging and oxygen evolution reactions at a positive electrode charging at potential E_{chg}, at two different temperatures, T_1 and T_2 ($T_2 > T_1$). i_{chg} and $i_{chg'}$ are the charge currents for the charged and discharged electrodes, respectively, and $i_{O_2T_1}$ and $i_{O_2T_2}$ are the oxygen evolution currents at T_1 and T_2, respectively. (Reprinted from Ref. [5].)

cell illustrate the change-over from an endothermic nature of the charge process to an exothermic reaction during overcharge. The higher the cell temperature, the earlier the charge reaction becomes exothermic, i.e. at 20 °C, the exothermicity sets in at ~80% of full charge, whereas at 0 °C, the reaction becomes exothermic at ~95% state-of-charge (SOC). The cell temperature is thus elevated during overcharge, which in turn results in a decrease in the cell voltage (due to its negative temperature coefficient of ~0.5 mV/°C [2,3]) and an increase in the overcharge rate (at constant charge voltage). Furthermore, the charge efficiency of the Ni electrode is low at high temperatures, due to the parasitic oxygen evolution process being more favorable, especially at high temperatures [4]. For example, the polarization curves for the oxygen evolution (Fig. 2 [5]) indicate a higher oxygen evolution reaction at higher temperatures. Also, the temperature coefficient of the equilibrium potential is lower in magnitude for the Ni reaction (−1.514 mV/°C) compared with the parasitic oxygen evolution reaction (−1.68 mV/°C) [2]. The increased oxygen evolution in turn generates further heat in the cell, eventually causing a thermal run-away. Constant voltage charge control is, therefore, inapplicable in critical applications, such as on spacecraft requiring high degree of safety and reliability. For example, on the LEO spacecraft, there is little time allowed for charging the battery, as compared with the Geosynchronous Earth Orbit (GEO) spacecraft. The Low Earth Orbit (LEO) battery is thus charged at a relatively higher rate, with the power from relatively large solar arrays; charge control is rather critical under these conditions to prevent thermal run-away. Efforts to develop an optimum charge methodology resulted in the use of temperature-compensated voltage limits during charging of batteries, under LEO conditions [6].

The purpose of the temperature-compensated voltage (V/T) limits is to achieve desired percent recharge ((Ah in/Ah out) × 100 or the inverse percent of cell throughput efficiency) across a range of battery temperatures. For sustained orbital operations, the percent recharge must be greater than 100%. Higher percent recharges, on the other hand, can affect the life of the battery. To achieve the desired percent recharge between these two limits under widely varying conditions (load variations, sun angles, eclipse times, etc.), a family of V/T curves have been developed by NASA for battery charging [6]. In this paper, we report the generation of such V/T curves for an aerospace Ni–Cd battery, based on a first-principles', mathematical model [7]. These models have been developed by Jet Propulsion Laboratory (JPL) in conjunction with Texas A&M University and the University of South Carolina. The original versions of the models were based on a macrohomogeneous description of the porous electrodes in the Ni–Cd cell, similar to those developed by Newman and Tiedeman [8] and Fan and White [9]. Current versions are based on the approximation of the porous electrode behavior to a homogeneous reaction layer, i.e. planar geometry. This approximation is valid due to the dominant nature of the diffusion and conduction processes in the solid matrix compared with that in the liquid phase [10,11]. The development of a battery model with all the relevant sub-routines and its prediction accuracy in relation to a practical aerospace battery have been described in Ref. [12]. The applicability of this homogeneous reaction (planar) approach has been demonstrated for selected spacecraft applications. Here, we demonstrate the applicability of this model to predict the V/T limits for an aerospace Ni–Cd battery. As may be seen below, the construction of the V/T curves from the experimental data is rather elaborate, expensive and often incomplete due to the sensitivity of the V/T limits to the orbit conditions (discharge/charge or occultation-day cycle) and cell design.

2. Experimental generation of V/T curves

There is not much of a documentation in the literature on the generation of the V/T curves, nor are the constraints on the application of these voltage limits well understood. For the sake of completeness and with the objective of providing details on the conditions for simulations, the method of constructing the V/T curves is briefly discussed below.

Historically, the voltage-limited charging was initially used in low-altitude orbit applications, with or without current limits depending on battery temperature and solar array characteristics. The design of such voltage-limited chargers involved considerable effort in current–voltage characterization, and in the design of electronic circuits that limit the battery voltage during charge. Particular attention is focused on the sensitivity of battery-system performance to slight changes in the level and slope of the battery voltage limit, and to changes in cell and battery characteristics with time and service. It was also realized that it was desirable to have different battery voltage limits in the latter stages of the mission from those in the early stages. Also, the use of a single battery voltage limit did not permit control of the battery's percent recharge, its heat generation during overcharge, nor did it compensate for a partial or complete cell short during

battery charge. Such considerations led to the present general practice of using multiple temperature-compensated battery voltage limits, each selectable by ground command.

Several controllable or measurable parameters, e.g. voltage limit, temperature, peak charge current or in-rush current (i.e the maximum charge current before the set charge voltage is attained), average cell voltage and depth-of-discharge, interact during cycling with voltage-limited charge control and thus determine the percent recharge, the taper current and the SOC. Also, the *I–V* characteristics of a cell are nonlinear with temperature and SOC so that it is only possible to evaluate accurately the total effect of the parameter changes by: (i) performing a matrix of tests under simulated spacecraft environment conditions, or (ii) performing simulations using *I–V* databases which have been previously developed by experiments.

As a first step in the construction of the *V/T* curves, discharge/charge cycles are performed on the sampled cell/battery under mission-simulated conditions. The duration of the discharge and charge phases, discharge current and the peak charge current are thus specified by the mission. The initial SOC depends on the prior history of the cell. However, for a given set of test conditions as described above, there will be a unique value for the initial SOC at which the percent recharge attains a steady-state value during cycling. Higher initial SOCs will result in a decrease in the percent recharge (or cell SOC) after each orbit cycle, whereas as at lower initial SOCs, there is an increase in the percent recharge (or cell SOC). Consequently, the percent recharge has to be measured after several cycles (e.g. 16 cycles), or after the percent recharge remains stable within 1% variation for three consecutive cycles. The percent recharges thus obtained at various charge voltage limits and at two different in-rush currents of 0.4 C and 0.25 C are plotted against the cell voltage, as in Fig. 3 [4]. Such percent recharge versus cell charge voltage plots are generated at various temperatures and in-rush currents relevant to the mission. Based on years of cell test data and experience with numerous flight programs, a range of percent recharge has been recommended at various temperatures for LEO applications (Fig. 4) [6]. The two curves in Fig. 4 are intended to bracket the acceptable recharge, with the upper limit being driven by limited thermal dissipation and the lower limit being that necessary to prevent capacity loss due to an incomplete charging. Increasing the depth-of-discharge or decreasing the charge rate would result in lower percent recharges. Conversely, increasing the initial SOC and increasing the charge rate would cause the percent recharges to increase. The voltage range corresponding to the bracketed percent recharge is divided into eight equal segments for the sake of convenience of the on-board electronics and are numbered accordingly. The lines joining the voltages corresponding to a given percent recharge at various temperatures (35 to −10 °C) constitute the *V/T* levels (Fig. 5(a) and (b)) [5,12,13]. Fig. 5(a) shows a family of the *V/T* curves developed by NASA [6,13], whereas Fig. 5(b) illustrates the family of *V/T* curves developed recently by GE Astrospace for an Ni–Cd battery on the Mars Observer Mission [14]. In the latter case, two levels (labeled as shifted and unshifted), each consisting of eight levels have been used for an improved control on the percent recharge. The *V/T* levels 1 and 2 in Fig. 5(b) are chosen to control the percent recharges in the charging of a 22-cell string containing one shorted cell. *V/T* level 8, on the other hand, is selected to provide a 'safe' operating voltage below the hydrogen evolution of cells and should be used with caution.

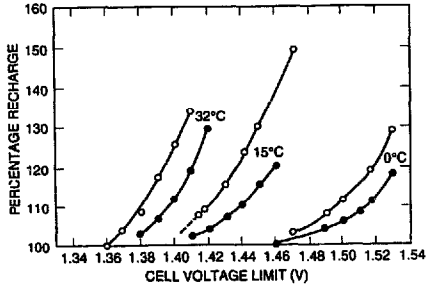

Fig. 3. Variation of percent recharge with the voltage limit for a 90-min LEO cycling (30 min discharge at 15% depth-of-discharge and 60 min charge on SAFT-America Ni–Cd cells at an in-rush current of (○) 0.4 C and (●) 0.25 C. (Reprinted from Ref. [4].)

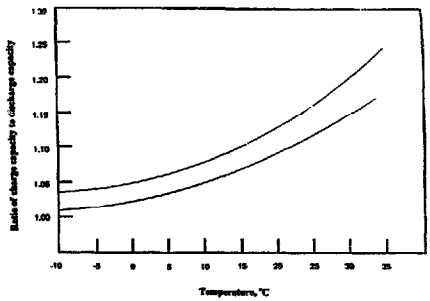

Fig. 4. Recommended charge/discharge ratio as a function of cell temperature.

3. *V/T* curves from the first principles' model

3.1. Outline of the model and test conditions

The *I/V* characteristics of an aerospace Ni–Cd cell have been simulated, using the mathematical model described earlier [11,12] and outlined briefly here. The model is built around principles of:

1. material balance for the dissolved species generated/consumed by the electrochemical reaction and transported by diffusion and migration;

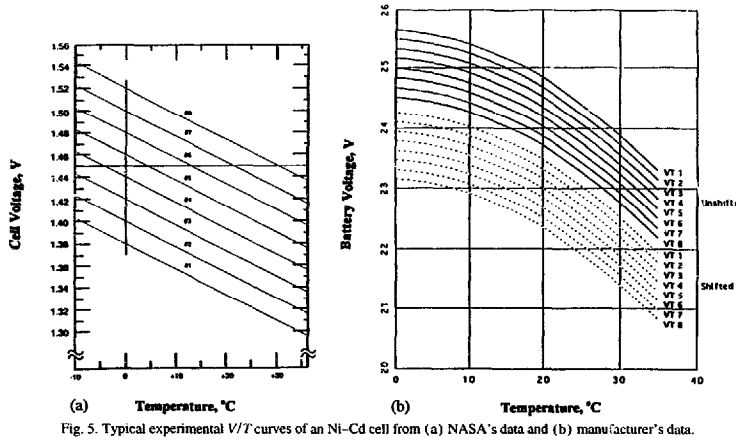

Fig. 5. Typical experimental *V/T* curves of an Ni–Cd cell from (a) NASA's data and (b) manufacturer's data.

2. changes in the electrochemical potential in the solid phase and in the electrolyte;
3. charge transfer kinetics through a modified Butler–Volmer rate equation;
4. principles of conservation of charge in the electrochemical cell, and
5. effects of intercalation and slow diffusion of protons into the positive electrode.

It is a simplification from the porous electrode models of Fan and White [9] in terms of recognizing the dominant effect of the mass transport processes in the solid phase compared with that in the liquid phase and thus assuming a uniform reaction layer (planar electrode). The model permits discharge/charge of any given cell under any specified test conditions, such as at constant current, constant voltage or constant power, with limits of either time, current, voltage or temperature. Furthermore, the recent model takes into account the existence of two phases of positive active material, i.e. β- and γ-forms of NiOOH and the corresponding reduced forms, β- and α-$Ni(OH)_2$ [15], for a more accurate prediction of the discharge and charge behavior.

For a simulation of the *V/T* curves, the parameters corresponding to a 50 Ah NASA standard Ni–Cd cell (50AB35), manufactured by Gates Aerospace Battery Division for the TOPEX (Topological Explorer) mission were used. The cell consists of 16 positives and 17 negatives of dimensions 11.5 cm × 11.5 cm. The simulated test regime is similar to a 90 min, LEO cycle, with a 30 min discharge to 15% depth-of-discharge followed by a 60-min of charge to a preset voltage limit, at two different in-rush currents of 0.4 and 0.25 C. Under these conditions, the experimental data on a typical aerospace Ni–Cd cell is availabie from in-house ground tests and in the literature, see Ref. [4]. These data will be used for a comparison with the simulations.

3.2. Simulations under LEO regime

Fig. 6(a) illustrates the variations of simulated cell potentials and cell current under such LEO regime at a charge voltage of 1.39 V, in comparison with the experimental data obtained using a boiler-plate cell, with a discharge rate of 0.75*C* (37.5 A), charge voltage limit of 1.44 V, and an in-rush current of *C*/2. The simulated curves are essentially similar to the experimental data on the boiler-plate Ni–Cd cell. The differences such as the sloping discharge profile may be attributed to the fact that the simulations correspond to a steady-state behavior, i.e. after repetitive cycling, whereas the experimental data reflects the behavior in early stages of cycling. The discharge voltages are higher for the simulations compared with the experimental data due to a higher discharge current in the latter case (0.75 C compared with 0.3 C for the simulations). The higher depth-of-discharge has also manifested in the observed cell voltage approaching the charge limit rather slowly compared to the simulations. Fig. 6(b) shows the simulated individual electrode potentials under the above LEO regime, which indicate that the polarization during discharge is mainly contributed by the positive electrode, the negative electrode exhibiting purely ohmic behavior. The output parameters of interest to the present study include percent recharge at the end of each cycle and the cell potential, individual electrode potentials, cell current, SOC of the cell and the charge efficiency. These simulations have been made under isothermal conditions.

3.3. Effect of state-of-charge

All the output parameters, especially the percent recharge, are strongly dependent on the SOC of the cell, or more specifically of the positive electrode. With low initial SOCs, the

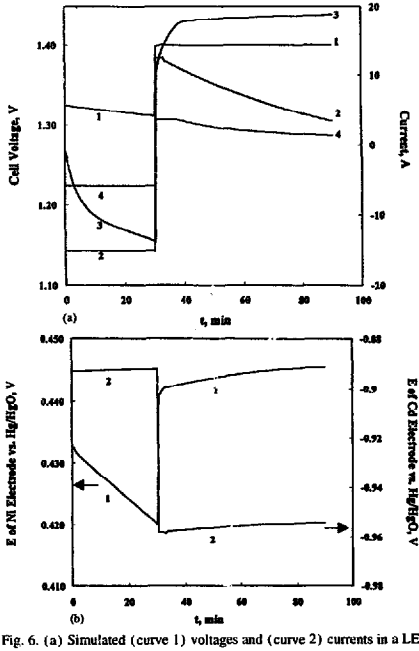

Fig. 6. (a) Simulated (curve 1) voltages and (curve 2) currents in a LEO cycle at 20 °C with a charge voltage limit of 1.39 V and in-rush current of C/4 compared with the experimental boiler plate (curve 3) voltages and (curve 4) currents with a charge voltage limit of 1.44 V and in-rush current of C/4. (b) The individual electrode potentials of (curve 1) NiOOH and (curve 2) Cd electrodes vs. Hg/HgO.

percent recharges are fairly low and continue to increase after each LEO cycle. With a high initial SOC, on the other hand, the percent recharge is initially high and shows a decrease after each cycle. The percent recharge eventually attains a steady-state value and remains unchanged after subsequent cycling. The steady-state value is a unique value for a given temperature and in-rush current. Fig. 7(a) and (b) illustrates the variations in the simulated cell voltages and currents during a LEO cycle, at six different values for the SOC, i.e. 0.4, 0.5, 0.6, 0.7, 0.8, and 0.9 at 20 °C with a charge voltage limit of 1.40 and in-rush current of 12.5 A. As may be seen from the figure, higher the initial SOC, faster would the cell approach the voltage limit during charge. Also, due to the charge voltages being high with high initial SOCs, the charge efficiency is reduced due to the accompanying oxygen evolution (Fig. 7(c)), resulting in a decrease in the SOC from the initial value (Fig. (7d)). At lower initial SOCs, on the other hand, the charge efficiency is higher and hence the increase in the SOC after each LEO cycle. Fig. 8 shows such a variation in the percent recharge after a LEO cycle, with the SOC of the cell. It is interesting to note that after 15 cycles, the percent recharge as well as the SOC attain steady-state values, which is consistent with the experimental methodology of allowing 16 LEO cycles for the percent recharge to stabilize [13].

3.4. Effect of in-rush current

In-rush current is another parameter affecting the percent recharge. As illustrated in Fig. 3, the percent recharge generally increases with an increase in the peak current. In order to examine the effect of the in-rush current on the predicted percent recharges, simulations have been carried out at seven different in-rush currents, i.e. 10, 12.5, 15, 17.5, 20, 22.5 and 25 A. Typical plots showing the cell potentials and cell currents during a LEO cycle at the above in-rush currents are shown in Fig. 9(a) and (b). A low charge voltage limit of 1.39 V was chosen for these simulations to examine the effect of in-rush current on the rechargeability of the Ni electrode, without much interference from the oxygen evolution process. At higher in-rush currents, the cell quickly approaches the voltage limit and gets into tapered current mode. At lower in-rush currents, on the other hand, the tapered current sets in later, but the charge return is also low, as evident from Fig. 9(c), which shows the variation of SOC during a LEO cycle at different in-rush currents. The amount of charge injected into the cell is thus low at low in-rush currents, increases with an increase in the in-rush current initially, and levels off later (Fig. 10). This is further illustrated in the percent recharge versus voltage limits plots at various temperatures, as detailed below. It may be pointed out here that our experimental tests on a TOPEX cell also indicate that the percent recharge increases with increasing in-rush currents [16].

3.5. Percent recharge-voltage limit relationships

Simulations have been performed in the above-mentioned LEO regime at two in-rush currents (0.25 and 0.4 C), at various cell voltages in a span of about 1 V and finally at different temperatures. As mentioned earlier, simulations had to be repeated several times under each conditions, in order to attain the steady-state percent recharge, i.e. for the initial and final SOC after one LEO cycle to be identical. Such plots correlating percent recharge with the voltage limit have been generated at temperatures of 0, 10, and 20 °C (Fig. 11). These plots are similar in shape and behavior compared with the experimental data in Fig. 3. However, the simulated percent recharges are found to be less sensitive to the changes in the in-rush current when compared with the experimental data. This is attributed to the fact that the voltage limit during charge is attained rather rapidly in the simulations, due to higher charge voltages predicted by the model, as discussed below. It is clear from Fig. 11 that the percent recharge expectedly increases with an increase in the voltage limit, more prominently after a specific voltage, e.g. 1.46 V at 20 °C. This specific voltage corresponding to the rapid increase

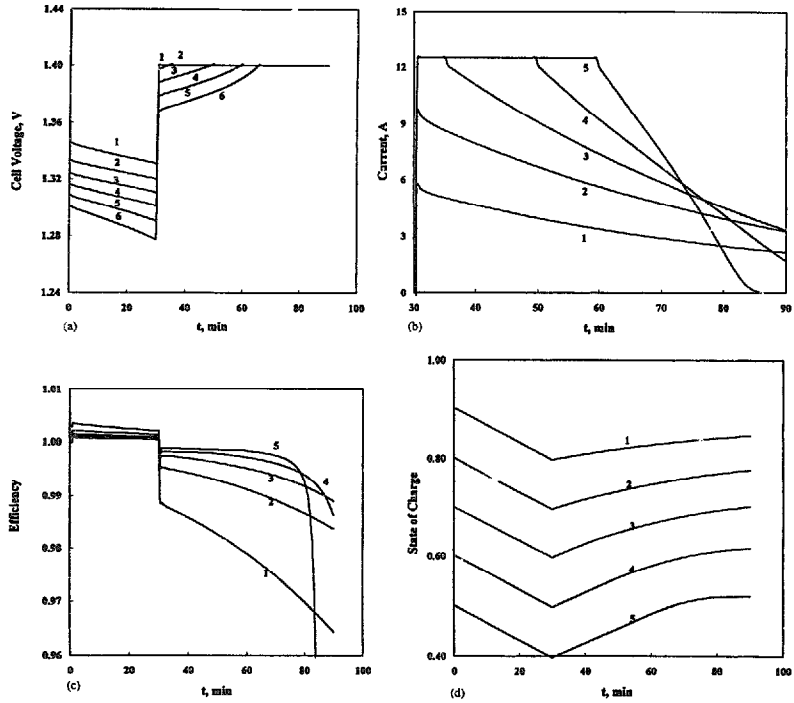

Fig. 7. Predicted (a) cell potentials, (b) currents, (c) efficiencies and (d) SOCs of an Ni–Cd cell during a LEO cycle with an initial SOC of (curve 1) 0.9, (curve 2) 0.8, (curve 3) 0.7, (curve 4) 0.6 and (curve 5) 0.5 (curve 6 in Fig. 7(a) corresponds to an SOC of 0.4) and with a charge voltage limit of 1.40 V and in-rush current of C/4 at 20 °C.

in the percent recharge is observed to increase with a decrease in the cell temperature. This is related to the negative temperature coefficient of the cell e.m.f. for the Ni–Cd cell. Furthermore, the SOC corresponding to the steady-state percent recharge increases with the voltage limit as well with the cell temperature, as shown in Fig. 12. Fig. 12 thus provides very useful information on what the SOC of a healthy cell would be on a repetitive LEO cycling with a specified voltage limit and at a specified temperature.

3.6. V/T curves from simulated percent recharge-voltage limit plots

Using the range of percent recharge at various temperatures identified from various flight data to be suitable for LEO applications (Fig. 4), a range of voltage limits has been identified at various temperatures. The voltage range determined from the model simulations corresponding to the bracketed percent recharge has been divided into eight segments. The lines joining the voltages corresponding to a given

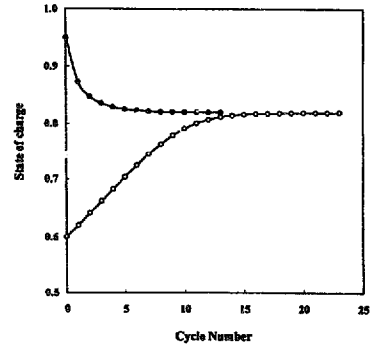

Fig. 8. Variation in the SOC, from an initial (●) high value and (○) low value during LEO cycling at 20 °C with a charge voltage limit of 1.39 and in-rush current of C/4.

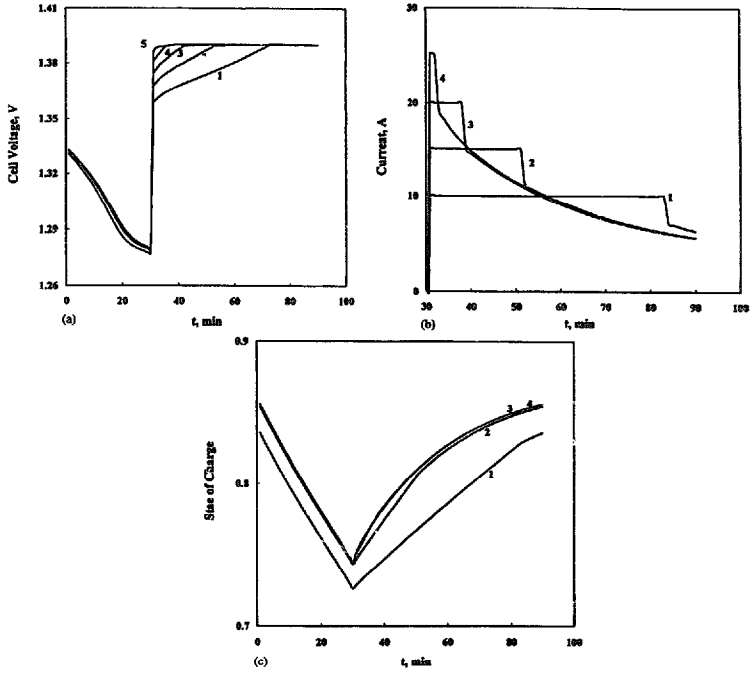

Fig. 9. Predicted (a) cell voltages, (b) currents and (c) SOCs of an Ni–Cd cell in a LEO cycle at 20 °C with a charge voltage limit of 1.39 V and various in-rush currents of (curve 1) 10, (curve 2) 12.5, (curve 3) 15 and (curve 4) 17, respectively. Curve 5 in Fig. 8(a) refers to an in-rush current of 20 A.

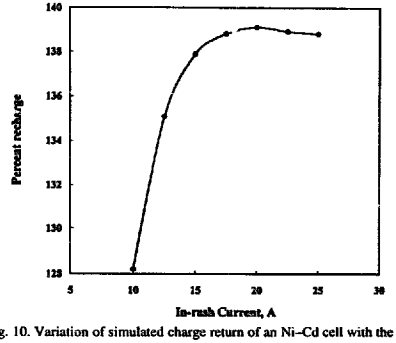

Fig. 10. Variation of simulated charge return of an Ni–Cd cell with the in-rush current in a LEO cycle at 20 °C with a charge voltage limit of 1.39 V as a function of in-rush current.

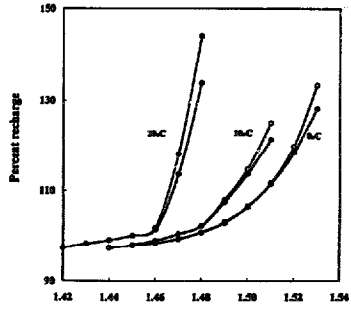

Fig. 11. Variation of simulated percent recharges with the voltage-limit for an Ni–Cd cell in LEO cycling, at temperatures of 0, 10 and 20 °C, and at in-rush currents of (●) 0.25 C and (○) 0.4 C, respectively.

percent recharge at various temperatures (0 to 20 °C) constitute the *V/T* levels. The *V/T* levels thus constructed between 0 and 20 °C are illustrated in Fig. 13.

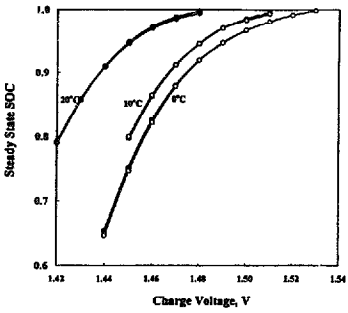

Fig. 12. Variation of steady-state SOC with the voltage limit at temperatures of 0, 10 and 20 °C and at in-rush currents of (●) 0.25 C and (○) 0.4 C, respectively.

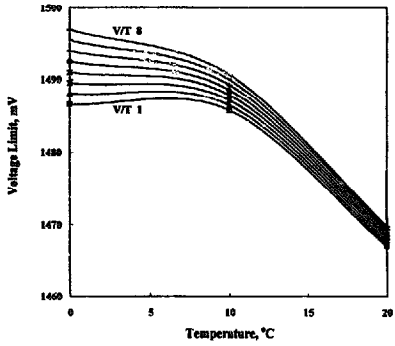

Fig. 13. Simulated V/T curves of an Ni–Cd cell in a LEO cycle.

3.7. Comparison of the simulated V/T curves with experimental data

A comparison of the simulated V/T curves with the experimental V/T curves (Fig. 5) in Refs. [6,13,14] reveals the following:

3.7.1. Shape of the V/T curves

The experimental V/T reported in Ref. [6] are linear and are a set of parallel curves in the range of -10 to $+30$ °C, with a slope of -2.33 ± 0.2 mV/°C. Interestingly, the slope is marginally higher in value compared with the temperature coefficient of the equilibrium cell potential, to account for the slower kinetics at low temperatures. The simulated V/T curves as well some of the recent experimental data (Fig. 5(b) [14]), on the other hand, tend to show non-linear behavior as a function of temperature. The non-linear behavior can be attributed to the non-linearity in the kinetics of oxygen evolution process with temperature. In other words, the kinetics of oxygen evolution are relatively suppressed compared with the Ni reaction, as illustrated in Fig. 2, such that lower voltage limits are sufficient to achieve complete charging of the cell at low temperatures. Consequently, the V/T curves are expected to bend to lower voltages at low temperatures.

3.7.2. Percent recharges

The percent recharges from the model are rather low for a given voltage. Alternately, the voltage corresponding to a given percent recharge is higher by about 20 mV. The poor recharging is due to the fact the initial cell charge voltages, after the switch-over from discharge are rather high, such that the cell approaches the tapered-charge mode rapidly. This also resulted in an insensitivity in the recharge percent to the in-rush current, i.e. the percent recharge is identical at two different in-rush currents unlike in the experimental data.

3.7.3. V/T range

The spread in the voltages from V/T level 1 to V/T level 8 is rather low. It is only ~20 mV (2.5 mV/level) at low temperatures as compared to ~140 (17.5 mV/level) observed experimentally. Under ambient conditions, it is even lower, about 10 mV (1.25 mV/level). This may once again be related to higher charge voltages from the model than observed experimentally. This aspect of higher predicted charge voltages is not as much evident in our earlier studies of the model, involving constant current charges instead of V/T charging and is currently being addressed.

4. Conclusions

Thermally-compensated voltage limits are the most suitable charge control parameters for an Ni–Cd battery to minimize overcharge in applications requiring rapid recharge, such as in LEO satellites. Experimental determination of these curves is rather tedious, also due to the specificity of the V/T curves to the mission orbit conditions and to the cell design. The V/T curves generated from first-principles' mathematical battery models are in general agreement with the experimental data in terms of their shape, and dependence on the SOC and in-rush current. The simulated V/T curves are non-linear with respect to temperature, similar to the data from GE Astrospace (Fig. 5(b)) but unlike the NASA curves (Fig. 5(a)). This is attributed to the improved charge efficiency of the Ni electrode at low temperatures. The simulations provide slightly higher charge voltages for the Ni–Cd cell, which results in a reduced percent recharge (at comparable voltage) or high voltage limit (for a comparable percent recharge), less sensitivity to the changes in the in-rush current and less voltage span corresponding to the desired range of percent recharge.

Acknowledgements

This work was carried out at the Jet Propulsion Laboratory, California Institute of Technology, under contract with the

National Aeronautics and Space Administration and was sponsored by NASA Chief Engineer's Office, as part of the NASA battery program.

References

[1] P. Bauer, Batteries for space power systems, *NASA Publication SP-172*, Washington, DC, USA, 1968.

[2] S.U. Falk and A.J. Salkind, *Alkaline Storage Batteries*, Wiley, New York, 1969.

[3] D.D. Macdonald and M.L. Challingsworth, *J. Electrochem. Soc., 140* (1993) 605.

[4] W.R. Scott and D.W. Rusta, Sealed-cell nickel–cadmium battery applications manual, *NASA Reference Publication 1052*, 1979, p. 82.

[5] N.C. Cahoon and G.W. Heise, *The Primary Battery*, Vol. 2, Wiley, New York, 1976.

[6] F.E. Ford et al., *NASA Reference Publication 1326*, 1994, p. 13.

[7] P.J. Timmerman, *Proc. 29th Intersociety Energy Conversion Engineering Conf., Monterey, CA, USA, 1994*, p. 112; P.J. Timmerman, S. Di Stefano, P.R. Gluck and D.E. Perrone, *Proc. 26th Intersociety Energy Conversion Engineering Conf., Boston, MA, USA, 1991*, p. 358; K. Clark, G. Halpert and P. Timmerman, *Proc. 24th Intersociety Energy Conversion Engineering Conf., Washington, DC, USA, 1989*, p. 1479; P. Timmerman, K. Clark and G. Halpert, *Proc. 23rd Intersociety Energy Conversion Engineering Conf., Denver, CO, USA, 1988*.

[8] J. Newman and W.H. Tiedeman, *J. AIChE, 21* (1975) 25; J. Newman, *J. Ind. Eng. Chem. Fundamentals, 17* (1978) 367–369.

[9] D. Fan and R.E. White, *J. Electrochem. Soc., 138* (1991) 17; *J. Electrochem. Soc., 138* (1991) 2952; Z. Mao and R.E. White, *J. Electrochem. Soc., 138* (1991) 3354; Z. Mao, P. De Vidts, R.E. White and J. Newman, *J. Electrochem. Soc., 141* (1994) 54; P. De Vidts and R.E. White, *J. Electrochem. Soc., 142* (1995) 1509.

[10] J. Weidner and P. Timmerman, *J. Electrochem. Soc., 141* (1994) 346.

[11] P.J. Timmerman and B.V. Ratnakumar, *Space Power Conf. Albuquerque, NM, USA, 17–20 Apr. 1995*.

[12] B.V. Ratnakumar, P. Timmerman, C. Sanchez, S. Di Stefano and G. Halpert, *J. Electrochem. Soc., 143* (1996) 803–812.

[13] W. Webster, *NASA Goddard Space Flight Center*, Jan. 1957 (cf. Ref. 3, p. 340).

[14] G. Perlman (GE Astrospace), personal communication.

[15] A.H. Zimmerman, *Proc. Symp. Hydrogen and Metal Hydride Batteries, 1994*, Vol. 94-27, The Electrochemical Society, Pennington, NJ, USA.

[16] F. Deligiannis, D. Perrone and S. Di Stefano, to be presented at the *Proc. 31st Intersociety Energy Conversion Engineering Conf., Washington, DC, USA, Aug. 1996*.